AD-A038 829 WISCONSIN UNIV-MADISON F/G 20/6
AN ALL-REFLECTION FOURIER TRANSFORM INTERFEROMETER FOR THE 500---ETC(U)
APR 77 F L ROESLER, D TRACY, D HUPPLER N00014-67-A-0128-0025
UNCLASSIFIED NRL -8094 NL

1 OF 1
AD A038829

END
DATE FILMED
5-77

NRL Report 8094

An All-Reflection Fourier Transform Interferometer for the 500- to 1000-Micrometer Wavelength Region

F. L. Roesler, D. Tracy, D. Huppler, and R. Fonck

University of Wisconsin

and

Mark Daehler and D. P. McNutt

Upper Air Physics Branch
Space Science Division

April 6, 1977

NAVAL RESEARCH LABORATORY
Washington, D.C.

SECURITY CLASSIFICATION OF THIS PAGE (When Data Entered)

REPORT DOCUMENTATION PAGE

READ INSTRUCTIONS BEFORE COMPLETING FORM

1. REPORT NUMBER: NRL Report 8094	2. GOVT ACCESSION NO.
3. RECIPIENT'S CATALOG NUMBER	
4. TITLE (and Subtitle): AN ALL-REFLECTION FOURIER TRANSFORM INTERFEROMETER FOR THE 500- TO 1000-MICROMETER WAVELENGTH REGION	5. TYPE OF REPORT & PERIOD COVERED: Final report on one phase of a continuing NRL Problem.
	6. PERFORMING ORG. REPORT NUMBER
7. AUTHOR(s): F. L. Roesler, D. Tracy, D. Huppler, R. Fonck, Mark Daehler, and D. P. McNutt	8. CONTRACT OR GRANT NUMBER(s): Contract ONR 0014-67-A-0128-0025
9. PERFORMING ORGANIZATION NAME AND ADDRESS: Naval Research Laboratory, Washington, D.C. 20375	10. PROGRAM ELEMENT, PROJECT, TASK AREA & WORK UNIT NUMBERS: NRL Problem A01-62
11. CONTROLLING OFFICE NAME AND ADDRESS: Department of the Navy, Office of Naval Research, Arlington, Va. 22217	12. REPORT DATE: April 1977
	13. NUMBER OF PAGES: 23
14. MONITORING AGENCY NAME & ADDRESS (if different from Controlling Office)	15. SECURITY CLASS. (of this report): Unclassified
	15a. DECLASSIFICATION/DOWNGRADING SCHEDULE

16. DISTRIBUTION STATEMENT (of this Report)

Approved for public release; distribution unlimited.

17. DISTRIBUTION STATEMENT (of the abstract entered in Block 20, if different from Report)

18. SUPPLEMENTARY NOTES

19. KEY WORDS (Continue on reverse side if necessary and identify by block number)

Diffraction grating
Far infrared
Interferometer

20. ABSTRACT (Continue on reverse side if necessary and identify by block number)

An all-reflection, two-beam interferometer has been designed, constructed, and tested. It may fill the need for a rugged, cryogenically coolable instrument for space applications. The interferometer uses a grating with symmetric grooves as a beam splitter. Each of the two arms contains a blazed grating with identical groove spacing to nullify the dispersion caused by the beam splitter. A model operated essentially as anticipated. An effect due to the asymmetric displacement of

(Continued)

DD FORM 1 JAN 73 1473 EDITION OF 1 NOV 65 IS OBSOLETE
S/N 0102-014-6601

SECURITY CLASSIFICATION OF THIS PAGE (When Data Entered)

380 100

20. Continued

the side gratings with respect to the beam splitter has been explained both theoretically and experimentally.

CONTENTS

PREFACE

The NRL Space Science Division has for many years been observing astronomical sources radiating in the far infrared. From these studies it has become apparent that a large-etendue instrument with moderate spectral resolution would offer significantly more valuable data than that obtainable from existing instruments, which were either of small etendue (grating-type spectrometers) or limited to broadband photometry. Although laboratory spectrometers exist in abundance, instruments that operate at liquid helium temperatures and can withstand the rigors of a rocket launch and a space environment are far less readily available.

In the search for suitable instrumentation, an all-reflection interferometer being developed at the University of Wisconsin offered the possibility of an extremely rugged instrument that could be cooled. The instrument was originally developed for the ultraviolet region of the spectrum, for which transmitting optical components are not available. With the prospect of applying these principles also in the far infrared, Professor Roesler undertook the responsibility for directing the design, construction, and test of such an instrument under contract ONR NO 0019-67-A-0128-0025. The work was done at Madison except for some of the tests, which were made in Washington because of the availability there of two microwave generators. This report contains the results of those studies and represents the final contract report. We believe the interferometer has been shown to be a potential candidate as a large-etendue interferometer for space applications.

AN ALL-REFLECTION FOURIER TRANSFORM INTERFEROMETER FOR THE 500- TO 1000-MICROMETER WAVELENGTH REGION

I. INTRODUCTION

Fourier transform spectroscopy with a Michelson interferometer is well known to offer two very significant advantages, especially in the infrared region of the spectrum, over conventional grating and prism spectroscopy. The first of these is the etendue advantage, which at a given resolving power gives the instrument much higher flux-handling capacity than conventional spectrometers. This advantage of axial fringe instruments is due to the large solid angle of light that can be accepted by the dispersing element without degrading resolution.

The second is the multiplex advantage, which may be realized when noise in the output signal is limited by detector-amplifier technology rather than by photon arrival statistics. In this case, noise in the output is not increased by detecting more light, so that the effective observing time for each wavelength interval is greatly increased by observing all wavelengths simultaneously.

However, in certain wavelength regions there are practical disadvantages to the conventional Michelson interferometer. Since the beam splitter is used in transmission, the instrument is limited to spectral regions for which transmitting materials are available. In the ultraviolet, the use of an LiF beam splitter would permit operation down to 1050Å, but it is not known how to manufacture from it large and perfect enough beam splitters for use in interferometry. The best fused silica has excellent optical working properties, but stops transmitting at about 1650Å. In the far infrared, a number of plastic materials, Mylar® and polyethylene for example, are suitable for beam-splitting. However, they present problems because of their lack of rigidity, especially away from the carefully controlled laboratory environment. Furthermore, in the submillimeter spectral range it is ultimately desirable to cool the entire instrument with liquid helium to avoid swamping the detector with background radiation generated by the mirror and beam splitter. This increases the difficulty of working with thin-film beam splitters, which become brittle and are likely to break when cooled.

The concept of the all-reflection interferometer was generated in response to the problems posed by transmitting beam splitters. It was recognized that gratings are tested routinely by comparing the wavefront of monochromatic light diffracted from a grating with a wavefront reflected from an optical flat, and that therefore a suitable grating or combination of gratings might form the basis of an all-reflection beam splitter. Furthermore, since gratings are solid, rigid elements, there should be no complications with cooling or structural rigidity.

Manuscript submitted December, 1976.

Some of the elements of all-reflection interferometry have been discussed in a series of published papers [1-3]. The basic idea is that if a grating with symmetrically cut grooves is illuminated at normal incidence, two symmetrically diffracted wavefronts leave the grating, as shown in Fig. 1. If these wavefronts are reflected back on themselves by mirrors M_1 and M_2, they are recombined at the grating and interfere constructively or destructively with each other, depending on the path difference. Thus a Michelson-like interferometer is formed; it may be scanned by translating one of the mirrors in a direction normal to its surface. However, because only one wavelength at a time can be reflected back on itself with this arrangement (each wavelength leaves the grating at a different angle and hence mirrors M_1 and M_2 can be normal to the rays of only one wavelength) it is not suitable for broadened interferometry.

This deficiency is corrected by the arrangement shown in Fig. 2, which employs additionally the conventional gratings G_2 and G_3 to cancel the dispersion introduced by beam splitter G_1. Rays of all wavelengths then strike mirrors M_1 and M_2 at normal incidence and are reflected back on themselves. Rays of different wavelengths follow slightly different paths, as shown in the figure, but that is of no essential consequence. The interferogram can now be generated by displacement of mirror M_1. Thus, this device has the essential characteristics required for all-reflection broadband Fourier transform spectroscopy.

The remaining sections of this report discuss details of the theory, construction, and tests of a device intended for use in the 500- to 1000-μm wavelength region.

II. ON-AXIS THEORY OF THE INSTRUMENT

A schematic of the all-reflection interferometer is given in Fig. 3. We assume that beam splitter grating G_1 has symmetrical grooves, so that the beam is symmetrically split. Grooves with an isosceles-triangular or sine-wave cross section meet this requirement. Groove spacing $d_1 = d_2 = d_3$ is the same for all three gratings. The faces of the gratings and of the two mirrors are all parallel, and we assume that the rulings of the

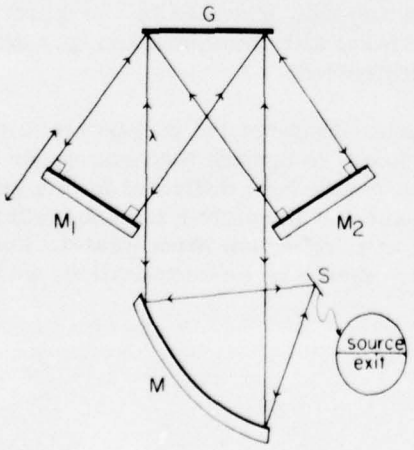

Fig. 1 — Schematic of a simple interferometer using a grating G to split a beam of light into two beams. Light goes from the source to the concave mirror M and then to the grating G. Mirrors M_1 and M_2 reflect the beams back to the grating, where they are recombined. Haidinger fringes are observed in the entrance aperture.

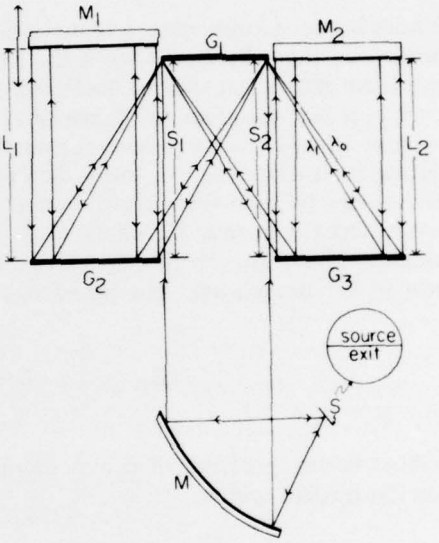

Fig. 2—All-reflection interferometer for use as a Fourier transform spectrometer. G_1, G_2, and G_3 are diffraction gratings with identical groove spacings. M_1 and M_2 are *plane front-surface mirrors*. Mirror M is a concave mirror. The path difference $\Delta = 2(L_1 - L_2)$ for normal-incidence rays is the same for the different wavelengths λ_0 and λ_1.

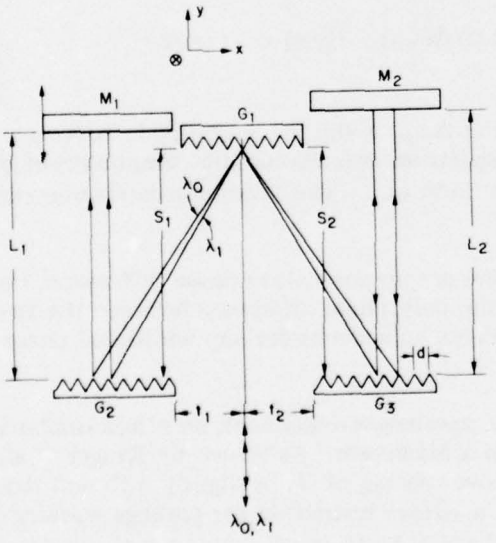

Fig. 3—All-reflection interferometer for use as a Fourier transform spectrometer. G_1, G_2, and G_3 are plane diffraction gratings with identical groove spacings. M_1 and M_2 are plane mirrors. At normal incidence, the path difference between the two arms of the instrument is $\Delta = (L_2 - L_1)$ for all wavelengths.

three gratings are all parallel. The side gratings are equidistant from the beam splitter; that is, $S_1 = S_2$. Finally, the two side gratings, needed to undo the dispersion of the beam splitter grating, are placed symmetrically in the x direction around a point of symmetry of G_1 such that $t_1 = t_2$ (e.g., a point of symmetry for the triangular-shaped grooves would be the tip or bottom of the groove).

Under these assumptions, a plane wavefront of wavelength λ is diffracted from G_1 in order k and then diffracted from the side gratings in the same order, so that the two beams hit the mirrors at normal incidence and retrace their paths out of the instrument. If $L_1 = L_2$, it is clear from the figure that the optical path difference between the two arms of the interferometer is zero for all wavelengths in all orders. Mirror M_2 is translated along its normal (i.e., in the y direction) to vary path length between the two beams. As can be seen from the symmetry of the device, the path difference between the two beams for normal incidence is $\Delta = 2(L_2 - L_1)$, which is independent of the wavelength. Thus, this instrument can be used as a broadband Fourier transform spectrometer in the usual way. The interferogram as a function of path difference is given by

$$I(\Delta) = \int_0^\infty B(\sigma)(1 + \cos 2\pi\sigma\Delta)\, d\sigma \,, \tag{1}$$

where $B(\sigma)$ is the spectrum of the incident light multiplied by the various efficiency factors for the optical system.

Spectrum $B(\delta)$ is given by the finite Fourier transform

$$B_c(\sigma) = \int_{-\Delta_{max}}^{\Delta_{max}} d\delta\, A(\Delta)[I(\Delta) - I(\infty)] \cos(2\pi\sigma\Delta) \tag{2}$$

where $A(\Delta)$ is the apodization function and Δ_{max} is the maximum path difference between the two arms of the instrument. Spectrum $B_c(\sigma)$ is usually computed numerically, with the integral in Eq. (2) replaced by a finite sum. The maximum resolution possible is $R = \sigma\Delta_{max}$.

The above equations assume that there are no anomalous phase differences between the arms of the interferometer. That is, the only phase difference between the two arms is given by $2\pi\sigma\Delta$. Care must usually be taken to account for any additional phase shifts [4].

If $S_1 \neq S_2$, the zero path position is wavelength-dependent, an effect similar to the misalinement of the compensating plate in a Michelson. As shown by Kruger et al. [1], the passband is severely limited if the groove spacing of G_1 is slightly different than that of the side gratings. However, this is not a serious restriction for gratings working in the far infrared. If $t_2 \neq t_1$ and $t_2 - t_1$ is not equal to an integral number of quarter-groove spacings, a wavelength-independent but order-dependent phase shift between the two beams may occur. This effect is discussed later.

In addition to the two interfering beams, an undiffracted beam resulting from specular reflection of the incident wavefront at G_1 is returned to the exit aperture. To

separate the two interfering beams from the undiffracted beam, the two side gratings are rotated by a small angle ξ around the χ-axis, as shown in Fig. 4. In this side view of the instrument, all rays are projected onto the yz plane. To locate the optic axis for the two interfering beams, we consider a ray lying in the yz plane and incident on G_1, making an angle α with the normal to G_1 and hence an angle $(\pi/2) - \alpha$ with the groove of G_1 that lies on the z-axis. This wavefront is partly reflected from G_1 and partly diffracted into order k. The reflected ray stays in the yz plane and makes an angle α with the normal to G_1 as it exits from the instrument. The diffracted ray comes out of the yz plane; its orientation is given by the pair of angles $(\psi, -\alpha)$, where $(\pi/2) + \alpha$ is the angle the diffracted ray makes with the z-axis (a groove of the grating) and ψ is the angle between the normal of G_1 and the projection of the diffracted ray onto the xy plane (the plane normal to G_1 and perpendicular to its grooves). The grating equation relates α and ψ by

$$k\lambda = d \sin\psi \cos\alpha .$$

For small ξ and α, the projection of this diffracted ray onto the yz plane makes an angle $\approx \alpha/\cos\theta$ with the y-axis, where we define $\sin\theta \equiv k\lambda/d$. This diffracted ray proceeds to the side gratings, hitting them at an angle $\approx [\pi/2 - (\alpha - \xi\cos\theta)]$ with respect to their grooves, and coming off the side gratings in a plane parallel to the yz plane. Since this angle is conserved, the rays hit the mirrors at an angle $\alpha - \xi(1 + \cos\theta)$ with respect to the normal to the mirrors, which are lines parallel to the y-axis. For the ray to return on itself (the definition of the optic axis), this angle must be zero, so the angle for the optic axis is given by

$$\alpha = \xi(1 + \cos\theta)$$

where $\cos\theta = \sqrt{1 - (k\lambda/d)^2}$ is a function of the wavelength and order number.

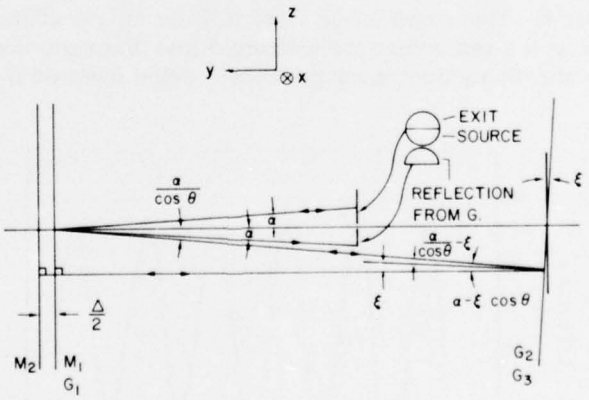

Fig. 4—Side view of the instrument, with side gratings tilted to separate the interfering beams from unwanted light reflected from beam splitter grating G_1

With a semicircular aperture of angular diameter β, the minimum ξ that is required to separate the interfering beams of interest from the reflected beam is given by $\alpha = \beta/4$. Hence the minimum tilt for the side grating is

$$\xi_{\min} = \frac{\beta/4}{1 + \cos\theta}.$$

Although setting $\xi \neq 0$ makes the position of the optic axis a function of wavelength and order number, which in turn decreases the etendue for wavelengths other than that to which the instrument is tuned, the advantage is that not only the undiffracted specular reflection from G_1 but also other unwanted beams of light in the instrument will not reach the exit aperture. (For example, any beam that bounces between a side grating and its corresponding mirror more than once, or any beam that, rather than exiting the instrument after returning to G_1, enters the opposite arm of the interferometer and then returns to come out off G_1.) Of course, the specularly reflected beam from G_1 is eliminated also. Hence if $\xi \geq \xi_{\min}$, only the interfering beams of interest enter the detector. The only unwanted light entering the detector will be that which leaves G_1 in order k and returns directly back to G_1 from G_2 and G_3 in order $2k$. The intensities of these beams can be minimized with the proper choice of blaze for G_2 and G_3.

For our experiments, $\cos\theta$ varies between 0.54 and 0.95 over the full wavelength range that passes through the instrument, and the shift of the optic axis for different wavelengths is enough to deteriorate the efficiency of the instrument somewhat. Nevertheless, most of the light from the interfering beams passes through the exit aperture to reach the detector.

Other factors affecting the efficiency of the instrument, such as blaze effects and the so-called walk-off effect, are discussed in detail by Kruger et al. [1] and are mentioned only briefly here. In particular, Fig. 5 shows the results of an approximate calculation of the efficiency of this instrument as a function of wave number σ, where σ_{Bk} is the blaze wave number in order k. This curve is Fig. 7 of Ref. 1. In the efficiency calculation, the fractions of light at a given σ that are diffracted into the various orders are given by examining the single slit diffraction envelope from a single facet of G_1. Light diffracted

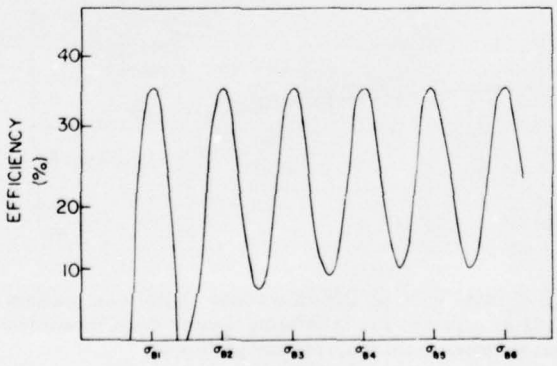

Fig. 5—Calculated efficiency as a function of wave number for an all-reflection interferometer, showing peaks of grating blaze wave numbers [1]

from G_1 in order k diffracts from G_2 (or G_3) also in order k. The amount of light leaving G_2 (or G_3) in order k is determined from the single slit diffraction envelope of the individual facets of G_2 (or G_3). The return path of the light through the instrument is treated in the same way, and the portion of light that proceeds through the instrument in order k is then estimated. In addition, the loss in intensity due to the walk-off effect and the contributions from all orders with significant efficiency for a given σ are included in this estimate. The important feature of this curve is the periodic peaking in efficiency at each blaze wave number.

Finally, even for $\xi \neq 0$, the on-axis rays still have a path difference $\Delta = 2(L_2 - L_1)$, although the obliquely incident rays have a somewhat more complicated path difference. The interference fringes are no longer circles, as they are for a Michelson interferometer, for which $\xi = 0$.

III. EXPERIMENT

An all-reflection interferometer has been constructed for operation in the far infrared. Top and side views of the optical system are shown in Figs. 3 and 4, respectively, and top and side mechanical views are shown in Figs. 6 and 7.

The gratings and mirrors were all made from aluminum on a milling machine. The beam splitter grating G_1 is 76 mm square, while the side gratings are 76 mm × 168 mm. Two sets of gratings were made and tested, one with a grating constant of $d = 3.81$ mm, the other with $d = 6.35$ mm. The beam splitter is a symmetric grating with triangular grooves having a facet blaze angle of 20°. Side gratings G_2 and G_3 have a conventional asymmetric profile and the same blaze angle of 20°. The mirrors are flat to at least $\lambda/20$ at a wavelength of 500 μm. For this test device (Fig. 3), $S_1 = S_2 = L_2 = 136$ mm.

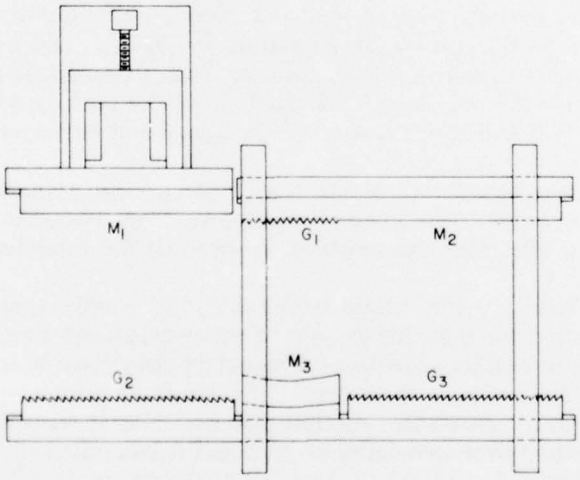

Fig. 6—Top view of the far-infrared all-reflection interferometer

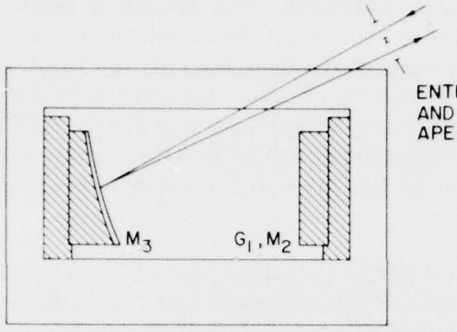

Fig. 7—Side view of the far-infrared all-reflection interferometer

The movable mirror M_2 can be translated along the normal to its surface. A stepping motor drives the mirror at 1.67 μm per step. The maximum possible displacement is 18.7 mm, which corresponds to a resolving power of $\approx$37 at λ = 500 μm.

The input and output beams are collimated by an off-axis paraboloidal mirror with a focal length of 26 cm. The side gratings are tilted by an angle ξ chosen so that the centers of the semicircular entrance and exit apertures are separated by 14 mm. Copper tubing 0.5-in. in diameter is used as light pipes to feed the light from the source to the entrance aperture and from the exit aperture to the detector. When a mercury arc lamp is used as the source, it is modulated by a mechanical chopper at a frequency of $\approx$173 Hz. The klystron source is electrically modulated. The detector is a liquid-helium-cooled InSb hot-electron bolometer whose signal is measured with a lock-in amplifier. With each step of the interferometer mirror, data are punched onto paper tape.

The fixed mirror M_1 and the gratings are supported by an aluminum yoke. Gratings G_2 and G_3, which are mounted on a common backing plate, were adjusted to be parallel to each other; then G_1 and M_1 (cut on the same piece of aluminum) and M_2 were all adjusted to be parallel to G_2 and G_3 by measuring S_1, S_2, L_1, and L_2 at the corners of the gratings and the mirrors with a vernier caliper. This alinement is good to $\pm$25 μm if carefully done. After the adjustment for parallelism, the backing plate for G_2 and G_3 was tilted to make $\xi \neq 0$ and thus separate the entrance and exit apertures.

The instrument was tested with klystron and mercury arc sources at NRL. The interferograms presented here were inverted using a standard two-sided complex finite Fourier transform (Eq. (2)) with the spectrum taken to be the modulus of the transform.

With a klystron having a wavelength of 3.2 mm, the interferogram was a single cosine curve, as expected for a Michelson-type Fourier transform spectrometer. Figure 8 shows the interferogram and its transform obtained by using two klystrons, with nominal wavelength of 3.2 and 2.2 mm, as the source. The resolving power is about 10 at 3.2 mm. As expected, the spectrum shows two discrete spectral lines at wave numbers of 4.65 and 3.16 cm^{-1}, corresponding to wavelengths of 2.15 and 3.16 mm.

In a second experiment, a hot mercury arc lamp was used as a broadband source. Two interferograms and their transforms, made with two sets of gratings with different groove spacings (d = 3.81 and 6.35 mm), are shown in Figs. 9 and 10. Both interferograms

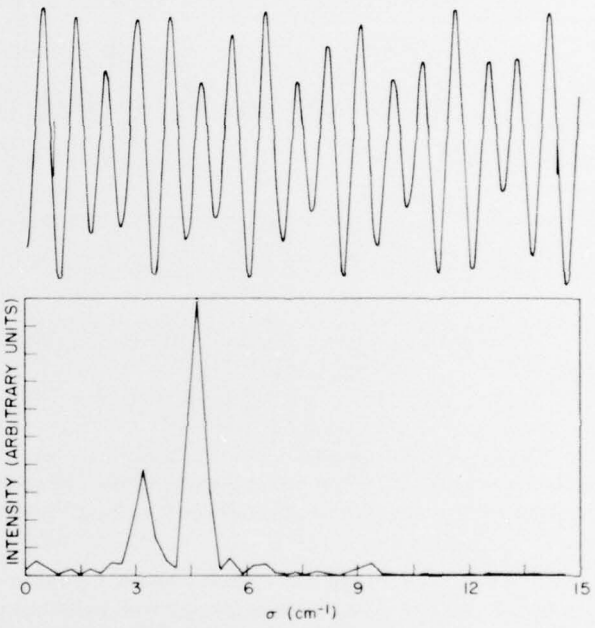

Fig. 8—(Above) Interferogram made using as source 2.2- and 3.2-mm klystrons simultaneously. Grating groove spacing, 6.35 mm; 512 data points; path difference between points, 67 μm. (Below) Spectrum obtained by double-sided transformation of interferogram. Peaks appear at 3.16 and 4.65 cm^{-1}, corresponding to wavelengths of 3.16 and 2.15 mm.

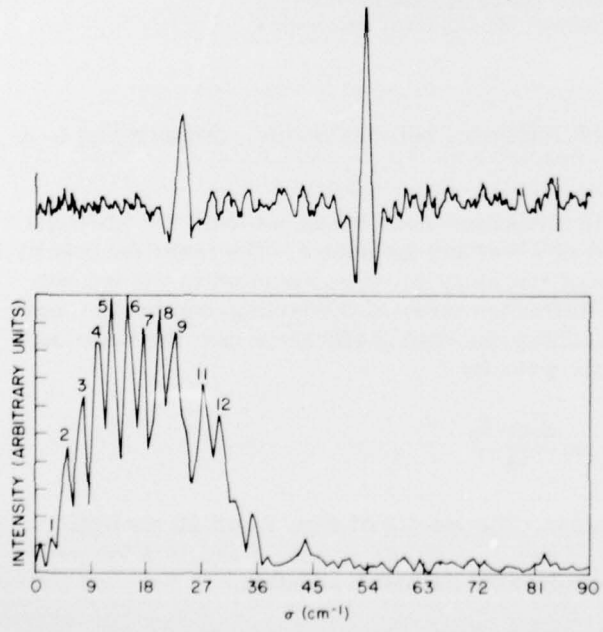

Fig. 9—(Above) Interferogram of a mercury arc source, made using gratings with groove spacing d = 6.35 mm. (Below) Transform of interferogram showing peaks due to periodic instrumental efficiency curve. The numbers identify each peak with a diffraction order.

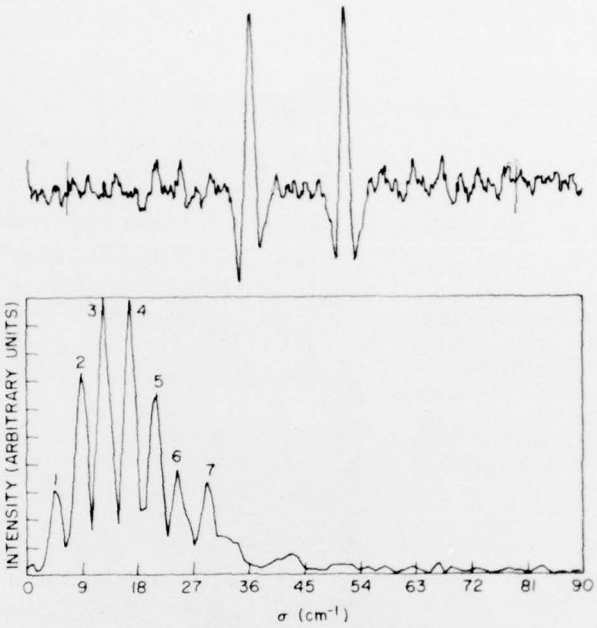

Fig. 10—(Above) Interferogram of a mercury arc source made using gratings with groove spacing d = 3.81 mm. The physical zero path-difference point lies approximately midway between the two large peaks. (Below) Transform of interferogram, showing peaks due to periodic instrumental efficiency curve. The numbers identify each peak with a diffraction order.

contained 512 points, with a 22.3-μm path difference between points, corresponding to a resolution limit of 0.877 cm^{-1}.

In each of Figs. 9 and 10 the spectrum contains many peaks, although the envelope of the peaks has the appearance expected of a mercury arc source. The peaks are present because of the structure in the instrumental efficiency curve, as discussed in the last section. Each peak corresponds to a single diffraction order of the grating, and its sharpness is due to the success of the blaze in maximizing the grating efficiency near the blaze angle θ_B. The wavelengths of peak efficiency are given by

$$\lambda_k = \frac{d \sin \theta_B}{k}$$

where k = 1, 2, 3, ... is the diffraction order. The spectra of Figs. 9 and 10 confirm that the spacing of the peaks does in fact depend on groove spacing d and that the wavelengths of peak efficiency agree quantitatively with the above equation.

None of the three interferograms shown has the appearance of the traditional Michelson interferogram, which is characterized by symmetry about a central maximum

located at the position of zero path difference. The interpretation of these interferograms, along with experimental data to confirm the interpretation, is presented in the next two sections.

An attempt was made to improve the efficiency at wavelengths away from the blaze wavelengths by replacing the side gratings with *split blaze* gratings. in which the grooves have a blaze angle of 15° in half the grating, and in the other half 25°. The groove spacing, $d = 3.81$ mm, is constant. Although this instrument gave the usual results for the two-klystron source, there was no signal detected above the noise level when the mercury arc source was used. The reason for this failure is not yet understood.

One further experimental difficulty should be mentioned. With the single klystron source, stationary mirror M_1 was blocked with an absorber and the path difference was scanned. The output signal shifted phase initially, but the resulting interferogram was still a cosine curve, indicating that some other interfering beams besides the beams of interest were reaching the detector. Most likely this output was due to interference between the light that hit movable mirror M_2 and the light that diffracted off beam splitter G_1, travelled to side grating G_2 or G_3, diffracted directly back on itself to return to G_1, and there recombined with the beam from M_2 to exit the instrument. Since the intensity of these beams from the side gratings in a Littrow mount is lower than that of the beams of interest, these unwanted beams of light are ignored in these preliminary studies.

IV. INTERPRETATION OF THE INTERFEROGRAMS

The observed asymmetry in the interferograms of Figs. 8 and 9 indicates an asymmetry in the two paths of the interferometer. Also, the fact that there is no central maximum at zero geometrical path difference in the interferogram of Fig. 10 suggests a large asymmetry. It is shown below that an asymmetry can be created by translating one of the gratings of the instrument in its own plane, normal to the grooves, and that the resulting phase errors are sufficient to explain the observations.

Lateral Translational Phase Shift Due to Grating Position

Consider a plane monochromatic wave incident on a plane diffraction grating. We use here the convention that the phase of the wavefront with respect to spatial coordinates is written as $\exp[i(\mathbf{K}\cdot\mathbf{x} + \Phi(\mathbf{X})]$, where $\mathbf{K}$ is the wave vector, $\mathbf{x}$ the spatial position vector, and $\Phi(\mathbf{x})$ describes any other residual phase shifts of the wavefront. For the incident plane wavefront, we take $\Phi(\mathbf{x}) = 0$. The diffracted wavefront will exhibit phase shifts that depend on groove shape and coating material and are functions of incident angle, wavelength, diffraction order, and polarization. For the grating beam-splitter arrangement considered in this report, the effects due to these phase shifts are considered minor due to the symmetry of the paths of the two beams. One large phase shift, due to the grating position alone, is of dominant importance. We call this the lateral translational phase shift (LTPS).

For a plane wave of wave number σ normally incident on a grating with groove spacing d, a plane wave is diffracted in order ℓ with an angle to the normal given by

$\ell = \sigma d \sin\theta$ (Fig. 11). We measure the relative phases of the incident and diffracted waves at P and P', respectively. If the grating is translated in its plane a distance ϵ perpendicular to its grooves in the direction of the diffracted beam, the diffracted wavefront is translated along with it, so that the phase of this wavefront relative to point P' is advanced by an amount $-2\pi\sigma\epsilon \sin\theta$.

In a completely equivalent manner, one could keep the grating stationary and translate the coordinate system, with its observation points P and P', a distance ϵ in the opposite direction and arrive at the same result.

Using the expression for $\sin\theta$, we have for the magnitude of the LTPS

$$\phi_\epsilon = |2\pi\ell\epsilon/d| \tag{3}$$

which is a function of the diffraction order but not of the wavelength. Since Eq. (3) has been obtained by considering only the far-field region of the wavefront, the LTPS is exactly linear in ϵ and is independent of the details of the groove shape. If $\epsilon = nd/\ell$, where n is an integer, the total shift is an integer multiple of 2π and the resulting phase between P and P' is indistinguishable from that prior to moving the grating.

In exactly the same manner as described above, one can show that Eq. (3) holds for the case of other than normal incidence and even oblique incidence. For the general case of an obliquely incident beam, let the unit vectors $\hat{\epsilon}$, $\hat{r}_\ell$, and $\hat{r}_0$ denote the direction of grating displacement, diffracted ray in order ℓ, and zero-order ray respectively. The sign of the LTPS is then given by

$$\text{sign}\,(\phi_\epsilon) = \text{sign}\,[\hat{\epsilon} \cdot (\hat{r}_0 - \hat{r}_\ell)]\ .$$

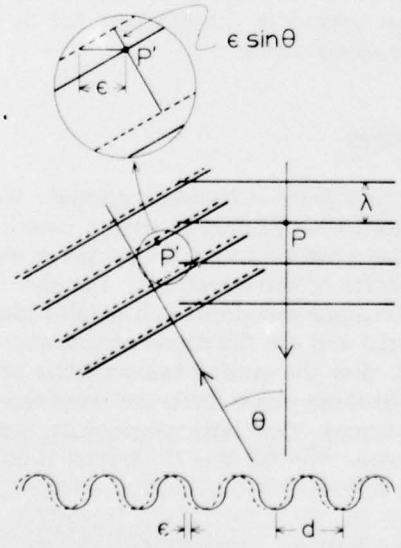

Fig. 11—Calculation of lateral translational phase shifts for normal incidence. When the grating is shifted to the left a distance ϵ, the diffracted wave pattern moves with it, resulting in a phase shift $2\pi\epsilon\sigma \sin\theta$, as measured between fixed observation points P and P'.

The sign can also be determined as follows. When the sense of the grating translation is the same as (opposite to) the direction of the diffracted wave relative to the zero-order ray, the phase change is negative (positive), which is equivalent to a decrease (increase) in the optical path of the beam.

Beam-Splitter Position Errors

The existence of lateral translational phase shifts (LTPS) implies that, if the grooves of the side gratings are not symmetrically located with respect to a normal plane of symmetry of the beam splitter grating (if it has one), then a phase error will arise from the difference in the lateral translational phase shifts of the two arms of the interferometer. We assume that the beam splitter grating has grooves with a symmetric cross-section and that the side gratings are mirror images of one another; if not, wavelength dependent errors are probably unavoidable.

In general, a misalinement of this type may be considered a lateral displacement of the beam splitter grating toward the fixed arm of the interferometer by a distance ϵ from the symmetry position. This displacement is equivalent to a displacement by a distance ϵ of both side gratings away from the fixed arm of the interferometer. Since each beam suffers a phase shift twice (once in the forward path, once in the return path), and the sign of the phase shift in the fixed arm is negative, the phase difference between the variable and fixed arm due to LTPS is given by

$$\phi_\epsilon(k) = \frac{8\pi k\epsilon}{d} \tag{5}$$

for each order of diffraction k (taken as positive) in which the interferometer is operating. Thus, for operation in diffraction order k, phase errors due to LTPS are not important provided that

$$\frac{\epsilon}{d} = \frac{n}{4k}, \quad n = 0, \pm 1, \pm 2, \ldots, \tag{6}$$

and for operation in two or more orders, there are no net effects, provided that

$$\frac{\epsilon}{d} = \frac{n}{4} \quad n = 0, \pm 1, \pm 2, \ldots. \tag{7}$$

Note that if $\epsilon/d = (2n + 1)/8$, then even diffraction orders have no net phase error, while odd orders suffer a net phase error of π.

The total phase difference between the two interferometer beams is then given by

$$\phi_T = \phi_\epsilon(k) + 2\pi\sigma\Delta \tag{8}$$

where $\Delta = 2(L_2 - L_1)$ is the geometrical path difference due to displacement of the movable mirror.

Interpretation of Data

In Sec. II it was noted that the efficiency of this instrument is a rapidly varying function of σ with sharp peaks at the blaze wave numbers, given by

$$\sigma_k = k/(d \sin \theta_B) , \qquad k = 1, 2, 3, \ldots .$$

The salient features of the observed interferograms may be understood by approximating this efficiency by a series of delta functions located at the σ_k. The total phase difference for the kth blaze wave number is given by

$$\phi_T = 2\pi k \sigma_1 (\Delta + 4\epsilon \sin \theta_B) . \tag{9}$$

For a broadband source, such that many orders of diffraction are being transmitted through the instrument, maxima of the interferogram occur only when all orders are in phase or when they differ by integer multiples of 2π. Thus peaks in the interferogram occur whenever

$$\sigma_1 (\Delta + 4\epsilon \sin \theta_B) = n \tag{10}$$

where n is an integer. This result, which is derived in the following more complete treatment, provides an explanation of the observed multiple peaks, their separation, and their displacement from the $\Delta = 0$ position.

Since the efficiency peaks have a substantial spectral width centered at the blaze wave numbers, a more realistic model for the instrumental efficiency curve is a convolution of an infinite series of equally spaced delta functions $D(\sigma)$ and a narrow spectral width $W(\sigma)$. Each delta function in $D(\sigma)$ corresponds to a blaze wave number, while $W(\sigma)$ represents the off-blaze efficiency effects of the three-grating beam splitter. It is assumed that $W(\sigma)$ is narrow enough that each wave number σ is transmitted through the instrument in only one order of diffraction. That is, the total width of $W(\sigma)$ is less than $\sigma_1 = (d \sin \theta_B)^{-1}$, which is the spacing between the delta functions in $D(\sigma)$. Spectrum $B(\sigma)$ is equal to the product of this efficiency and an overall envelope $E(\sigma)$, which is due to the Hg lamp white light spectral distribution, the detector efficiency, the efficiency of the auxiliary optics, etc. We have

$$D(\sigma) = \sum_{k=-\infty}^{\infty} \delta(\sigma - k\sigma_1) \tag{11}$$

$$B(\sigma) = [D(\sigma) * W(\sigma)] \cdot E(\sigma) \tag{12}$$

where the $*$ denotes a convolution and $k\sigma_1 = \sigma_k$ is the blaze wave number in order k.

When the phase error ϕ_ϵ due to the LTPS is not an integral multiple of 2π, the modulated term in Eq. (1) must be modified to take ϕ_ϵ properly into account; the interferogram is given by

$$I(\Delta) - I(\infty) = \int_0^\infty B(\sigma) \cos (2\pi\sigma\Delta + \phi_\epsilon) \, d\sigma \tag{13}$$

which we write as

$$I(\Delta) - I(\infty) = \frac{1}{2}\int_{-\infty}^{\infty} B(\sigma)e^{i\phi_\epsilon}e^{i2\pi\Delta\sigma}\,d\sigma\,. \tag{14}$$

Since $I(\Delta)$ is real, $B(\sigma)e^{i\phi_\epsilon}$ is taken to be a complex symmetric function of σ [5].

Using the convolution theorem and Eq. (12) in Eq. (14) results in

$$I(\Delta) - I(\infty) = \frac{1}{2}\left[\bar{W}\cdot\overline{(De^{i\phi_\epsilon})}\right] * \bar{E} \tag{15}$$

where $\bar{g}$ denotes the complex Fourier transform of a function g. The $\overline{(De^{i\phi_\epsilon})}$ factor is the interferogram that would result from an ideal interferometer with a complex spectrum given by $D(\sigma)e^{i\phi_\epsilon}$. From Eqs. (10) and (11), this factor is given by

$$\overline{(De^{i\phi_\epsilon})} = \sum_{k=-\infty}^{\infty} e^{i2\pi k\sigma_1(\Delta + 4\epsilon\sin\theta_B)}$$

where the summation index k denotes diffraction orders. The Poisson summation formula gives

$$\overline{(De^{i\phi_\epsilon})} = \frac{1}{\sigma_1}\sum_{m=-\infty} \delta\left(\Delta + 4\epsilon\sin\theta_B - \frac{m}{\sigma_1}\right). \tag{16}$$

The output of the instrument becomes

$$I(\delta) - I(\infty) = \frac{1}{2\sigma_1}\left[\bar{W}\cdot\sum_m \delta\left(\Delta + 4\epsilon\sin\theta_B - \frac{m}{\sigma_1}\right)\right] * \bar{E}\,. \tag{17}$$

The interferogram described by Eq. (17) is a series of equally spaced peaks whose positions are given by

$$\Delta_m = \frac{m}{\sigma_1} - 4\epsilon\sin\theta_B \tag{18}$$

which is simply the result obtained earlier in Eq. (10). The intensities of the peaks are modulated by $\bar{W}$, which is due to the nonzero efficiency of the three-grating beam splitter for σ near the blaze wave numbers. The profile of the peaks is given by $\bar{E}$. The spacing between peaks is given by

$$\Delta_{m+1} - \Delta_m = d\sin\theta_B \tag{19}$$

and the $m = 0$ peak is shifted from the $\Delta = 0$ position by

$$\Delta_0 = -4\epsilon\sin\theta_B\,. \tag{20}$$

The coarse features of the recorded interferograms in Figs. 9 and 10 are just those of the interferogram described by Eq. (17). Apparently, the three-grating beam splitter is so efficient off-blaze that only two or three peaks are detectable in the interferogram above the noise level. That is, $\overline{W}$ is so narrow that only a few peaks have a nonzero intensity in $I(\Delta)$.

The separation of the peaks in the interferogram, which depends simply on the periodicity of the blaze wave numbers, is proportional to $\sin\theta_B$, where θ_B is the on-blaze diffraction angle. The values of θ_B obtained by applying Eq. (19) to the interferogram peak spacing data are given in Table 1. These values of θ_B, deduced from the interferograms of Figs. 9 and 10, are to be compared to 40°, the value for which the gratings were designed.

The symmetry of the interferogram of Fig. 10 is explained if one assumes that $\epsilon/d = (2n + 1)/8$, with n an integer, so that successive diffraction orders have phase shifts differing by π. If this occurs, the geometrical zero path position should be located directly between the two peaks, which is what is observed.

Only a considerably smaller deviation of ϵ/d from a symmetry value of $n/4$ is required to explain the interferogram of Fig. 9. Using Eq. (20) and observing our sign conventions, one can easily deduce that the beam-splitter grating must have been displaced slightly away from the variable arm of the interferometer. The construction and alinement procedures for this experiment (Sec. III) were such that values of ϵ/d up to at least $\pm 1/4$ were possible.

Effect of LTPS on Inversion Procedures

For grating beam-splitter interferometers operating in a single order k, the effect of a lateral grating translation is to introduce a constant phase error, given by Eq. (5). Such a phase error is easily taken care of by standard methods [5], such as the use of the two-sided Fourier transforms. The same statement applies to simultaneous operation in several nonoverlapping orders, where the phase error is effectively a slowly varying function of wave number σ.

Unfortunately, when several overlapping orders are in use (i.e., two or more orders propagate through the instrument and interfere for one wave number), then both the instrument efficiency and, unless the alinement is perfect ($\epsilon = 0$), the phase error can be expected to show rapid and large variations with changing wave number. The details of

Table 1—Path Difference Separations of Interferogram Peaks and the Diffraction Angles Calculated from These Path Differences

d (mm)	Interferogram	$\Delta_{m+1} - \Delta_m$ (observed) (mm)	θ_B (calculated) (deg)
3.81	Fig. 10	2.39	38.85
6.35	Fig. 9	3.97	38.70

this effect are beyond the scope of this report, but it can be said to introduce substantial difficulties in the operation of a grating beam-splitter interferometer in high orders, unless the resolution is very high (where the rapid variations could be resolved) or very low (where they are unimportant).

V. EXPERIMENTAL VERIFICATION OF LATERAL TRANSLATIONAL PHASE SHIFTS

To test the validity of the above interpretation of the early experimental results of Figs. 8, 9, and 10, the interferometer was modified so that ϵ could be varied by translating the beam-splitter grating (G_1) and stationary side mirror (M_3) assembly in the plane of G_1 and in a direction perpendicular to the grooves of the grating. The position of G_1 and M_3 was varied with a micrometer drive to an accuracy of ±0.0001 in. (0.00254 mm). The value of ϵ could be varied up to a maximum of $1.5\,d$. For all the results reported in this section, the d = 0.15 in. (3.81 mm) gratings were used. Unless specifically mentioned, all other parameters of the experiment were essentially the same as reported in Sec. III.

With the 2.2-mm klystron as a source, the output of the interferometer was monitored as ϵ was varied to check the existence of an LTPS. The results are shown in Fig. 12. For this data, $\Delta \approx -0.3$ mm. As is evident, the output does not have a pure sinusoidal dependence on ϵ, but rather the amplitude of the basic sinusoidal behavior is modulated. Peaks 2 and 4 in this data correspond to the cases in which the point of symmetry of G_1 is the top and bottom of the triangular grooves respectively. The lower amplitude peaks, 1, 3, and 5 in the figure, correspond to the point of symmetry being

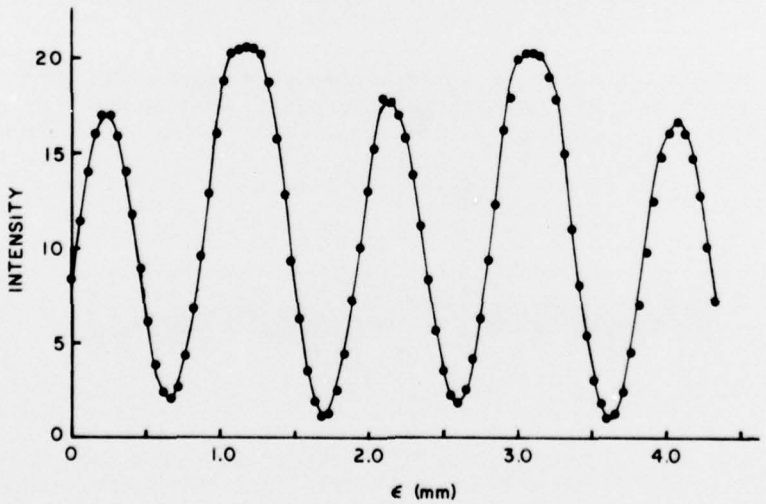

Fig. 12—Interferometer output as a function of λ for a 2.2-mm klystron source. Grating groove spacing is 3.81 mm, and path difference between beams is δ = −0.3 mm. For this case the ϵ = 0 position is not a symmetry position. A maximum occurs whenever $\Phi_T = 2\pi n$.

a midpoint between the top and bottom of the groove cross-section. The cause of this amplitude modulation is not clear, but it may be the fact that the wavefront reconstruction of the gratings is poor. That is, due to the relatively large ratio of wavelength to instrument dimensions, it is not strictly correct to assume that the wavefronts are plane waves after diffracting from the gratings.

However, these measurements clearly verify the existence of an LTPS. The average period in terms of ϵ between the peaks in Fig. 12 is 0.965 ± 0.025 mm, while Eq. (6) predicts a value of 0.952 mm for the change in ϵ between maxima (the λ = 2.2 mm signal is diffracted into first order only).

The interferograms obtained when the Hg lamp was used as a white light source were very dependent on the value of ϵ. The results for two cases are shown in Figs. 13 and 14. Figure 13 shows the resulting interferogram when ϵ was adjusted so that G_1 was placed very close to a point of symmetry. For reference, we say $\epsilon = 0$ for this case. Figure 14 shows the same situation, but with $\epsilon/d = 0.026$. The $\epsilon/d = 0$ case is fairly symmetric around the $\Delta = 0$ position and shows three peaks in the interferogram, while the $\epsilon/d = 0.026$ case shows three peaks that are not symmetric in intensity around the central peak, and all three peaks are displaced, with respect to $\Delta = 0$, from their positions in Fig. 13. Both these results are to be compared to Fig. 10, where $\epsilon/d \approx 0.125$ and only two peaks are seen, with both being approximately equidistant from the $\Delta = 0$ position. The peak positions of Fig. 10 have been duplicated by setting $\epsilon/d = 0.125$ with the modified apparatus.

In all, 10 white light interferograms were taken with different ϵ settings. The peak positions relative to a fixed value of Δ were measured as a function of ϵ from $\epsilon/d = 0$ to $\epsilon/d = 0.302$. The results of these measurements for the two peaks (2 and 3) are given in Fig. 15, where the peak position is plotted as a function of change in ϵ. The data fit a

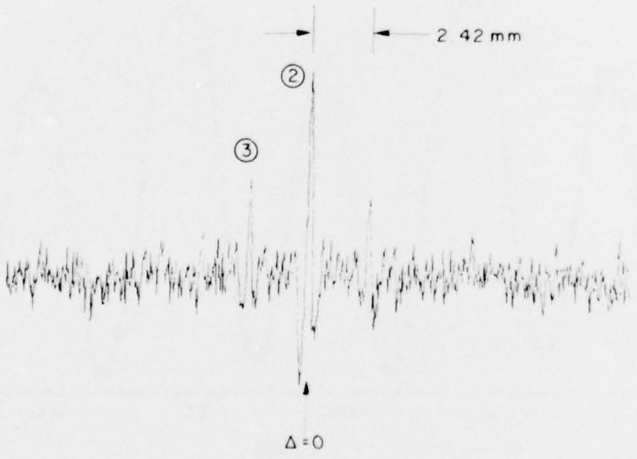

Fig. 13—Interferogram of a mercury arc source with $\epsilon = 0$, made using gratings with groove spacing $d = 3.81$ mm. The approximate $\Delta = 0$ position is shown by the arrow. Adjacent peaks are separated in path difference by 2.42 mm. The number labels of the peaks correspond to the labels in Fig. 15.

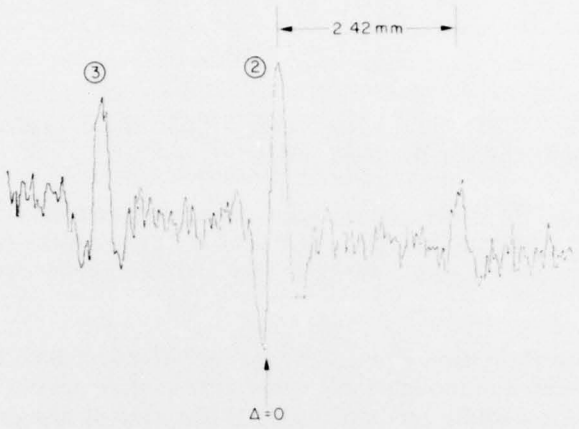

Fig. 14—Interferogram of a mercury arc source with $\epsilon = 0.026$ and groove spacing $d = 3.81$ mm. The peaks are shifted from their position in Fig. 13. The number labels of the peaks correspond to the labels in Figs. 13 and 15.

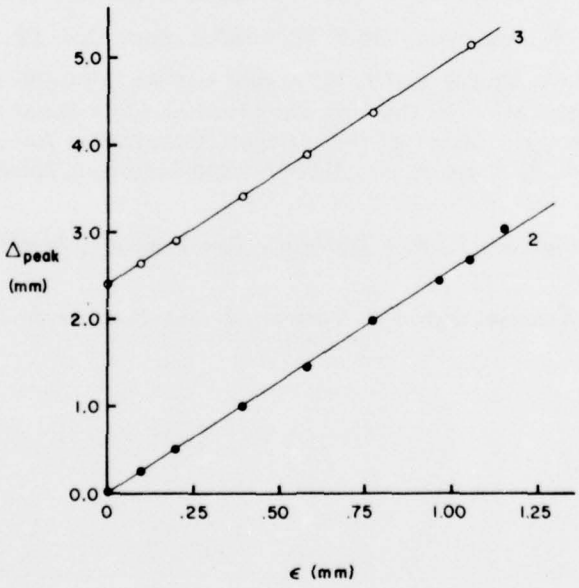

Fig. 15—Interferogram peak positions, measured by the path difference Δ between interfering beams, as a function of ϵ

straight line very well for both peaks. The origin of the vertical axis is arbitrary, but the slope of both lines is predicted by Eq. (18) to be

$$\frac{d(\Delta_m)}{d\epsilon} = -4 \sin \theta_B \, . \tag{21}$$

For $\theta_B = 40°$, $4 \sin \theta_B = 2.57$, while a least-squares fit to the data gives a slope of 2.59 for the peak 2 data and 2.60 for the peak 3 data.

From a total of 10 Hg White light interferograms, the average separation between adjacent peaks in terms of path difference is 2.42 ± 0.01 mm, while for $\theta_B = 40°$, Eq. (19) gives a predicted value of 2.45 mm. Again, theory and experiment are in reasonable agreement.

In conclusion, the expression in Eq. (18) for the effect of the LTPS in this interferometer has been verified, although some other effects were present. The simple model presented in Sec. IV successfully predicts the basic behavior of instrument. In particular, the movement and separation of the peaks in the interferogram are in quantitative agreement with theory.

REFERENCES

1. R. A. Kruger, L. W. Anderson, and F. L. Roesler, *J. Opt. Soc. Amer.* **62**, 938 (1972).

2. R. A. Kruger, L. W. Anderson, and F. L. Roesler, *Appl. Opt.* **12**, 533 (1973).

3. F. L. Roesler, R. A. Kruger, and L. W. Anderson, "An All-Reflection Interferometer with Possible Application in The Vacuum Ultraviolet," in *Space Optics: Proceedings of the Ninth Internatl. Congr. of the Internatl. Commission for Optics* (IX), B. J. Thompson and R. R. Shannon eds, ISBN 0-309-02144-8, p. 355-366, National Academy of Sciences, Washington, D.C., 1974.

4. R. W. Bell, *Introductory Fourier Transform Spectroscopy*, Academic Press, New York, 1972.

5. H. Sakai, G. A. Vanasse, and M. L. Forman, *J. Opt. Soc. Amer.* **58**, 84 (1968).